NTIA Report TR-13-494

Free-Field Measurements of the Electrical Properties of Soil Using the Measured Reflection Coefficient at Normal Incidence and Multilayer Analysis

February 2013

report series

U.S. DEPARTMENT OF COMMERCE • National Telecommunications and Information Administration

NTIA Report TR-13-494

Free-Field Measurements of the Electrical Properties of Soil Using the Measured Reflection Coefficient at Normal Incidence and Multilayer Analysis

Nicholas DeMinco
Paul M. McKenna
Robert T. Johnk
Chriss A. Hammerschmidt
J. Wayde Allen
Linh P. Vu

U.S. DEPARTMENT OF COMMERCE

February 2013

DISCLAIMER

Certain commercial equipment and materials are identified in this report to specify adequately the technical aspects of the reported results. In no case does such identification imply recommendations or endorsement by the National Telecommunications and Information Administration, nor does it imply that the material or equipment identified is the best available for this purpose.

CONTENTS

Page

1 Introduction.....1

2 Reflection Coefficient Measurement System 3

2.1 DRH Monostatic Measurement System.....3

3 Single and Multilayer Reflection Coefficient Analysis for a Stratified Earth 9

4 Electric Field Penetration Depth of the Soil 22

5 Conclusions.....25

6 References.....26

FIGURES

Figure 1. (a) Dual-ridge horn boresighted on ground target. (b) Dual-ridge horn antenna boresighted straight up. 3

Figure 2. Setup for Building A4 parking lot for measurement of ground constants. 4

Figure 3. Setup for Building A4 parking lot for calibration measurement reference over aluminum sheet. 5

Figure 4. Signal processing sequence to isolate the target reflection. 6

Figure 5. (a) Time-domain reflectometer plot with the DRH boresighted at an aluminum sheet. (b) Time-Domain reflectometer plot with the DRH boresighted straight up. 7

Figure 6. (a) Background-subtracted time-domain reflectometer plot with the DRH boresighted at the center of the aluminum sheet. (b) Time-gated plot with room and residual reflection effects removed by time gating. 8

Figure 7. The deconvolution process. 8

Figure 8. Multilayer structure of the ground for the multilayer analysis. 10

Figure 9. Measured data taken in May of 2011 for position 4 at Building A4. 12

Figure 10. The deconvolved impulse response envelope from measured data obtained from a Hilbert Transformation for position 4 at Building A4. 13

Figure 11. A plot from the multilayer prediction model that almost matches the measured data waveform of Figure 9. 14

Figure 12. A plot from the multilayer prediction model that compares to Figure 11 and shows insensitivity to changes in conductivity, σ, of the second layer. 15

Figure 13. A plot from the multilayer prediction model that compares to Figure 11 and shows insensitivity to changes in conductivity, σ, of the first layer. 15

Figure 14. Final plot from the multilayer prediction model with parameters for a 5.1 cm (2 inch) asphalt actual layer thickness. 17

Figure 15. Measurement setup for Building A4 parking lot with location of Positions 1, 2, 3, and 4. 18

Figure 16. Reflectivity measurement for four positions at Table Mountain Building A4 parking lot. 18

Figure 17. Impulse response envelope obtained from Hilbert Transform for four positions at Table Mountain Building A4 parking lot. 19

Figure 18. Measured data in the middle of Plateau Road taken in May 2010. 20

Figure 19. The deconvolved impulse response envelope from measured data in the middle of Plateau Road taken in May 2010. Note the dominant reflection from the air/ground interface. 20

Figure 20. Predicted reflectivity versus relative permittivity ε_r of the soil using the multilayer model in single layer mode with an assumed conductivity of 1.0 mS/m. 21

Figure 21. Skin depth for 1/*e* E-field attenuation versus frequency for various media types. 24

Figure 22. Skin depth for 1/*e* E-field attenuation versus frequency for various media types expanded to show lower frequencies. 24

FREE-FIELD MEASUREMENTS OF THE ELECTRICAL PROPERTIES OF SOIL USING THE MEASURED REFLECTION COEFFICIENT AT NORMAL INCIDENCE AND MULTILAYER ANALYSIS

Nicholas DeMinco, Paul M. McKenna, Robert T. Johnk,
Chriss A. Hammerschmidt, J. Wayde Allen, Linh P. Vu[1]

This report describes a free-field radio frequency (RF) measurement system that is currently being developed by engineers at the Institute for Telecommunication Sciences (NTIA/ITS). The objective is to provide estimates of the electrical properties of the ground (permittivity and conductivity) over which the measurement system is deployed. This measurement system uses reflection coefficient measurements at normal incidence over ground using a dual-ridged horn antenna placed close to and radiating directly down at the ground at specific antenna heights. Soil properties are extracted by comparing measured data with known analytical models for single and multilayer scenarios using optimization.

Key words: antenna; radio-wave propagation; deconvolution; Fourier transform; frequency domain; gating; dual-ridged horn antenna; reflectivity, signal processing, S-parameters, time domain; transmission loss; propagation measurement

1 INTRODUCTION

A near-earth propagation measurements program was initiated at the Institute for Telecommunication Sciences (NTIA/ITS) Table Mountain Field Site (TMFS) in May 2010 under the sponsorship of the Table Mountain Research Project. We continued this program in June 2011 with a second set of measurements. The purpose of these efforts was to determine the ground constants at the TMFS. While comparing measured and modeled results, questions arose about the assumed dielectric permittivity and conductivity of the soil at the TMFS. These ground constants can have a significant influence on RF propagation predictions near the ground and need to be accurately characterized. This led to the development of the measurement system described in this report.

The system described in Section 2 of this report performs reflection coefficient measurements of the ground surface at various locations at TMFS using a dual-ridged horn antenna. This analysis will concentrate on two sets of measurements. The first was conducted in May 2010 along Plateau Road at various road positions. The second set of measurements, taken in June 2011, was performed in the parking lot at Building A4 with a blacktop surface using stepped-frequency reflection coefficient measurements over a band of interest extending from approximately 700 MHz to 6000 MHz. For the set of measurements taken at Building A4, there is strong evidence

[1] The authors are with the Institute for Telecommunication Sciences, National Telecommunications and Information Administration, U.S. Department of Commerce, Boulder, CO 80305.

of multilayer ground behavior; the measurements taken along Plateau Road exhibit single layer behavior. The dual-ridged horn antenna was located at a fixed distance of 1.5 meters above ground, which corresponds to a 10.0 nanosecond round trip propagation time between the ground and the antenna. Section 2 describes the measurement system used to obtain the reflection coefficient. Section 3 describes the analysis performed and presents the equations used for the multilayer analysis along with the results of the analysis and measurements. Section 4 describes the electric field penetration depth of the soil. Section 5 contains the conclusions.

2 REFLECTION COEFFICIENT MEASUREMENT SYSTEM

The system, a schematic of which is shown in Figure 1, uses a vector network analyzer (VNA) to perform stepped-frequency reflection coefficient (S-parameter) measurements over a wide frequency range for the ground surface at TMFS. It employs a dual-ridged horn (DRH) antenna at a distance of 1.5 meters above the ground. The DRH antenna is mounted on a fiberglass mast and pointed directly at the ground surface below the antenna for the actual measurement. The DRH antenna can be rotated to point either at the sky or at the ground, which is a key feature in the calibration of this system.

The VNA is configured to perform stepped-frequency measurements of the antenna input reflection coefficient, which is the S-parameter S_{11}. Measurement data were acquired over a frequency range from 300 kHz to 6 GHz (in 300 kHz steps). Data for the analysis was extracted from this measurement set over a frequency range subset of 700 MHz to 6 GHz, corresponding to the operational frequency range of the DRH antenna.

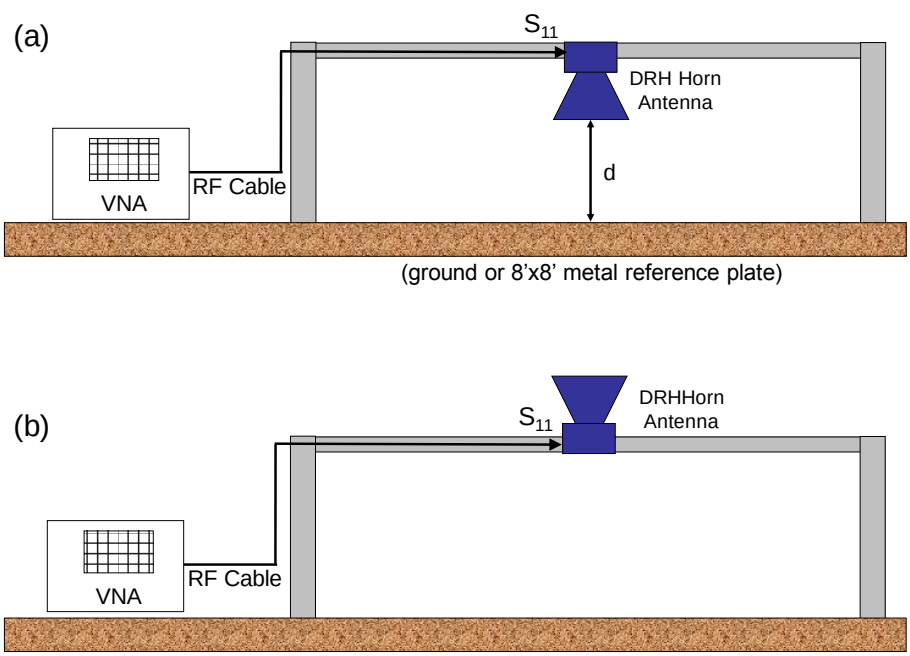

Figure 1. (a) Dual-ridge horn boresighted on ground target. (b) Dual-ridge horn antenna boresighted straight up.

2.1 DRH Monostatic Measurement System

The antenna is mounted on a rotatable fiberglass mast, which is supported by two dielectric carts. This configuration allows the DRH to be pointed straight up or straight down (Figure 2). A vector network analyzer, configured for one-port reflection coefficient measurements, is connected to the antenna input port through a section of 50 ohm coaxial cable. A full one-port calibration is performed by connecting precision standards to the end of the cable. The calibration allows us to measure the complex reflection coefficient. The resulting S_{11} data are referenced to the antenna input port, with the cable and VNA effects mathematically removed by the calibration. S_{11} is the complex input reflection coefficient of the antenna. Stepped-frequency

S-parameter magnitudes and phases are acquired over the frequency range of 300 kHz–6 GHz at evenly-spaced intervals of 300 kHz for a total of 20,000 points per sweep. The bandwidth capability of the DRH antenna limits the useful data to a band that extends from 700 to 6000 MHz. The data are then transferred to a computer for post processing.

Figure 2. Setup for Building A4 parking lot for measurement of ground constants.

The antenna and support structure are placed either over a section of ground or over an 2.5 m x 2.5m (8'x8') aluminum reference plate that acts as a calibration target (Figure 3), and the reflectivity at normal incidence is extracted from a two-part measurement sequence. The beamwidth of the antenna is approximately 45 degrees (worst case at the low frequency of 700 MHz), so for a one meter antenna height the aluminum reference plate sees a plus or minus 0.4 meter illumination with respect to the center of the plate, and is effectively an infinite ground plane. Time gating during the signal processing removes the edge effects of the aluminum reference plate and is not an issue. The aluminum plate provides a known reflection coefficient from a well characterized material at normal incidence. The antenna is bore-sighted straight down at the ground (normal or vertical) as is shown in Figure 1(a), and stepped-frequency one-port reflection data are acquired. The background measurement is performed by aiming the DRH antenna straight up as shown in Figure 1(b) and recording the stepped-frequency background data. This system exploits the directional characteristics of the DRH to permit effective background vector subtractions. The test setup provides minimal movement of the RF cables with excellent stability.

Figure 3. Setup for Building A4 parking lot for calibration measurement reference over aluminum sheet.

The surface reflections are isolated by invoking the signal processing steps shown in Figure 4. The goal of signal processing is to isolate the reflections from either the ground or metal plate reference and to provide the backscatter coefficient (*BC*), which correlates closely to the plane-wave reflection coefficient of the ground at normal incidence with a polarity reversal [1]. The first step is to perform a vector subtraction of the complex (magnitude and phase) background $S_{11_background}(f)$ from the complex, ground-boresighted (target) result denoted by $S_{11_target}(f)$. This procedure provides a background measurement of the clutter, which is subtracted from the subsequent measurements in order to improve the dynamic range of the measurement and unmask the target response. A "target" can either be bare ground or an aluminum metal sheet that is used for calibration purposes. The aluminum sheet is a well known analytically tractable solution, which allows the proper scaling of the magnitude and phase responses of the conductivity and dielectric constants of the ground. This step nearly eliminates the artifacts that are common to both measurements. The S-parameter that results from the subtraction is denoted by $S_{11s.}$ As a result, the antenna internal reflections are removed and environmental reflections external to the antenna are left over. The rest of the post-processing consists of two elements: filtering and gating. Filtering conditions the signal and eliminates out-of-band effects. Gating is used to enhance and isolate and suppress undesired scattering and radio interference. The objective is to isolate the ground reflection with minimized spurious effects.

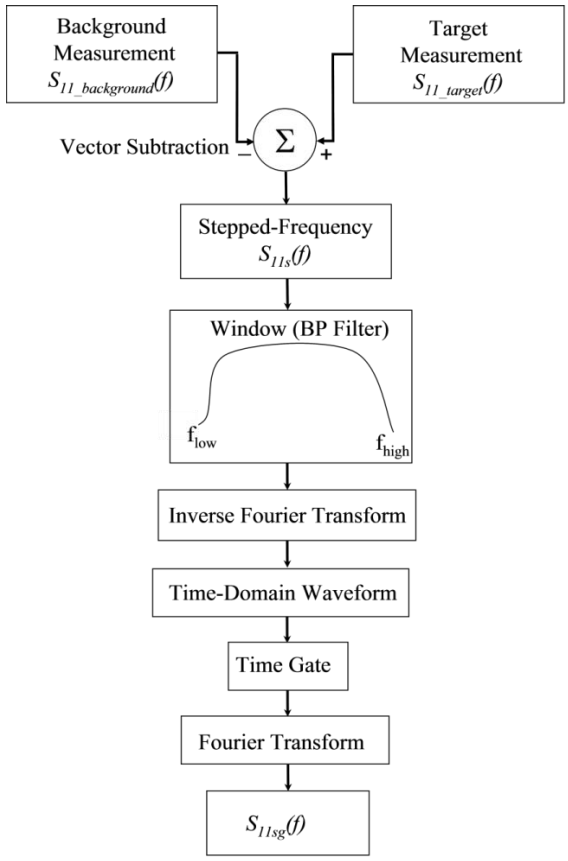

Figure 4. Signal processing sequence to isolate the target reflection.

The vector-subtracted signal is windowed to condition the signal and eliminate undesired out-of-band effects. The window is basically a bandpass filter with low-pass and high-pass cutoff frequencies f_{low} and f_{high}, A Kaiser-Bessel window [2] is used because it allows a wide variety of window shapes which are governed by a variable window index β. The windowing also significantly reduces an artifact of the mathematical manipulation known as Gibbs' ringing that occurs in transforming to the time domain. The data are then inverse Fourier transformed to the time domain. The result is a waveform that has the three primary components. The first component is the residual antenna reflection that remains after the vector subtraction. The second component is the primary reflection off the ground, and the third component is due to spurious packets that result from unwanted reflecting objects and scatterers in the vicinity of the test setup. Figure 5 shows a sequence of time-domain waveforms obtained from this process with the DRH placed above a 2.5 m × 2.5 m (8' × 8') aluminum sheet. Figure 5(a) shows the resulting waveform with the antenna pointed at the center of the aluminum sheet, and Figure 5(b) depicts the background waveform with the DRH pointed up at the sky. The internal antenna reflections are virtually identical in both cases.

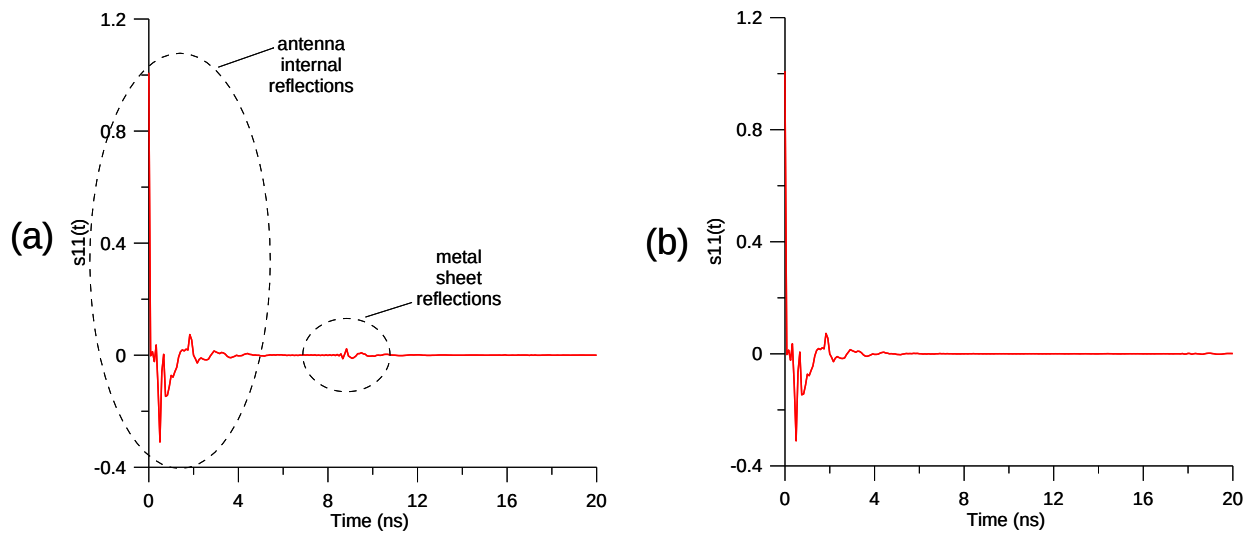

Figure 5. (a) Time-domain reflectometer plot with the DRH boresighted at an aluminum sheet. (b) Time-Domain reflectometer plot with the DRH boresighted straight up.

The reflection from the metal plate is visible when the antenna is pointed down, but is not there in the background measurement. This is due to the directional characteristics and the high-front-to-back characteristics of the DRH. The subtracted waveform is shown in Figure 6(a). In this case, the first waveform packet is the internal residual antenna reflection. The next packet is due to the reflection from the metal sheet, followed by spurious environmental reflections. Time gating is next applied to eliminate the residual internal and environmental reflections. The time gate is basically a rectangular window with start and stop times that are chosen to capture the reflection from the ground target, and eliminate the other scattering events. The gated ground reflection is then Fourier transformed to obtain the gated spectrum, $S11_{sg}(f)$, which is the final product of this process. Figure 6(b) shows the time-gated metal sheet reflection with the undesired components removed.

The gated frequency-domain reflectivity data for the ground patch and metal sheet are further processed using deconvolution [3]. This process is shown in Figure 7. The first step consists of a complex division of the gated ground patch data by the gated metal sheet reference. This normalizes the data and provides a direct comparison of the ground patch data with those of the metal sheet reference. In addition, the multiplicative antenna transfer functions cancel out, removing nearly all of the antenna effects [1]. The resulting data are referred to as the backscatter coefficient, *BC(f)*. A complex distance correction is next applied which accounts for both magnitude and phase changes produced by unequal heights in the ground patch and metal reference sheet measurements. These data are then windowed to suppress undesired interference and spurious out-of-band antenna responses. These data now correlate closely with the Fresnel plane-wave coefficient at normal incidence, over the operational frequency range of the DRH antenna. The primary difference between the backscatter coefficient and the plane-wave reflection coefficient is a sign reversal due to the reflecting properties of the metal sheet. An inverse Fourier transform is then applied to the windowed data, and the result is a high-resolution time-domain backscatter coefficient, *bc(t)*, with the antenna impulse response removed.

Both magnitude and phase information are acquired, which permits transformations to and from the time and frequency domain. This capability provides more insight into the reflection properties of the reflected wave over the ground and permits processing to enhance accuracy and signal fidelity by windowing the stepped frequency data and time-gating the time domain waveform.

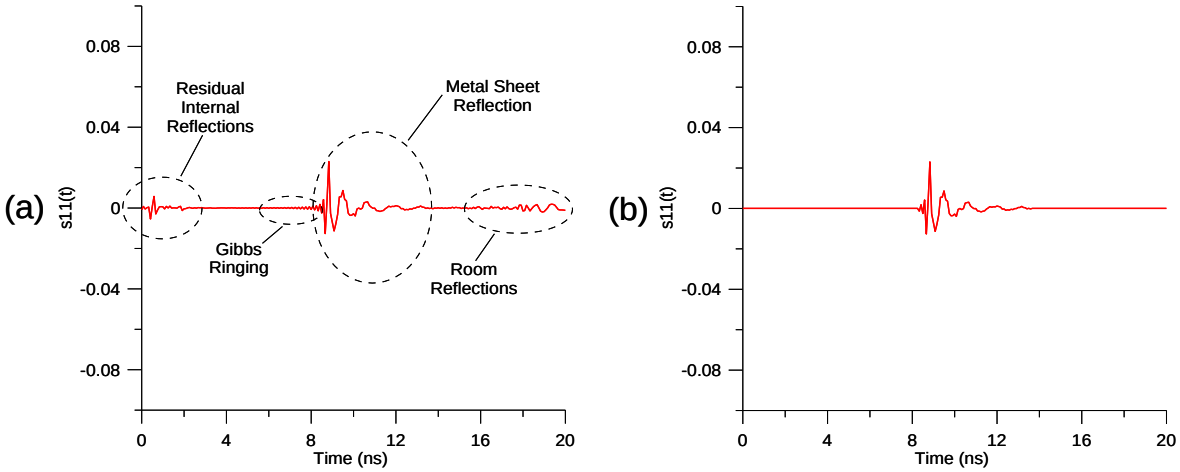

Figure 6. (a) Background-subtracted time-domain reflectometer plot with the DRH boresighted at the center of the aluminum sheet. (b) Time-gated plot with room and residual reflection effects removed by time gating.

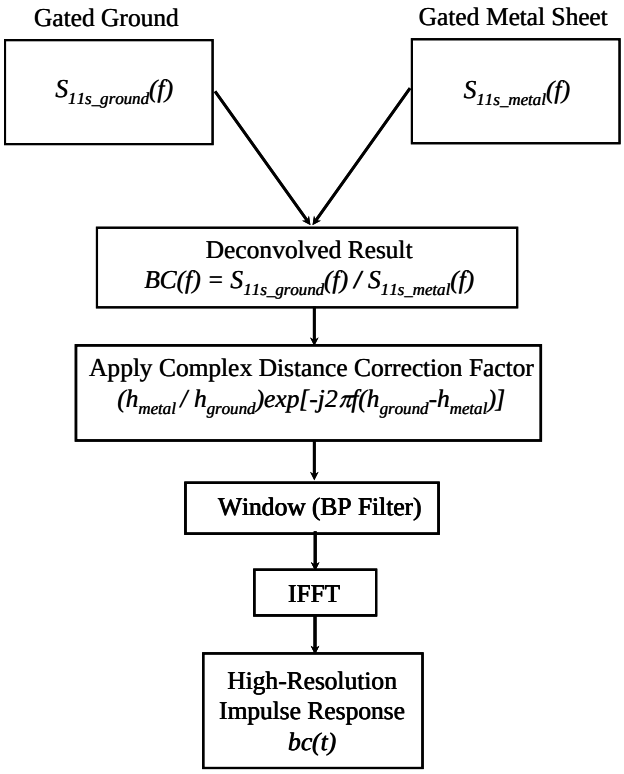

Figure 7. The deconvolution process.

3 SINGLE AND MULTILAYER REFLECTION COEFFICIENT ANALYSIS FOR A STRATIFIED EARTH

The ground constants were determined by using the reflection coefficient measured at the locations at the TMFS and comparing it to the predictions from the multilayer analysis computer code developed at ITS for a variety of ground constants and layer thicknesses. The approach was to compute the reflection coefficient of the multilayer structure for a variety of ground constants, layer thicknesses, and frequencies and match the measured reflection coefficient waveform to the predicted waveform curves to obtain the various ground constants.

R_v is the complex reflection coefficient for one layer for vertical polarization and is given by [5]:

$$R_v = \frac{\left(\varepsilon_r - i\frac{\sigma}{\omega\varepsilon_0}\right)\sin\psi - \sqrt{\left(\varepsilon_r - i\frac{\sigma}{\omega\varepsilon_0}\right) - \cos^2\psi}}{\left(\varepsilon_r - i\frac{\sigma}{\omega\varepsilon_0}\right)\sin\psi + \sqrt{\left(\varepsilon_r - i\frac{\sigma}{\omega\varepsilon_0}\right) - \cos^2\psi}} \tag{1}$$

where

ω is the angular frequency and is equal to $2\pi f$;
f is the radio frequency in Hertz;
μ is the magnetic permeability of the Earth, $\mu = \mu_r \cdot 4\pi \cdot 10^{-7}$ henries per meter;
μ_r is the relative permeability of the Earth;
$\varepsilon = \varepsilon_r \cdot \varepsilon_0 = \varepsilon_r \cdot 8.85 \cdot 10^{-12}$ = the permittivity of the Earth in Farads per meter;
ε_r is the relative permittivity of the Earth;
ε_0 is the permittivity of free space in Farads per meter;
σ is the conductivity of the Earth in Siemens per meter;
ψ is the angle representing the direction of the incident wave measured with respect to the Earth's surface.

At normal incidence (ψ = 90 degrees) (1) becomes:

$$R_v = \frac{\left(\varepsilon_r - i\frac{\sigma}{\omega\varepsilon_0}\right) - \sqrt{\varepsilon_r - i\frac{\sigma}{\omega\varepsilon_0}}}{\left(\varepsilon_r - i\frac{\sigma}{\omega\varepsilon_0}\right) + \sqrt{\varepsilon_r - i\frac{\sigma}{\omega\varepsilon_0}}}. \tag{2}$$

For the multilayer ground scenario at normal incidence we have N layers that have a finite thickness and ground constants sandwiched between two semi-infinite media. We have an air layer above the first ground layer and a semi-infinite layer L of Earth below the Nth layer as shown in Figure 8.

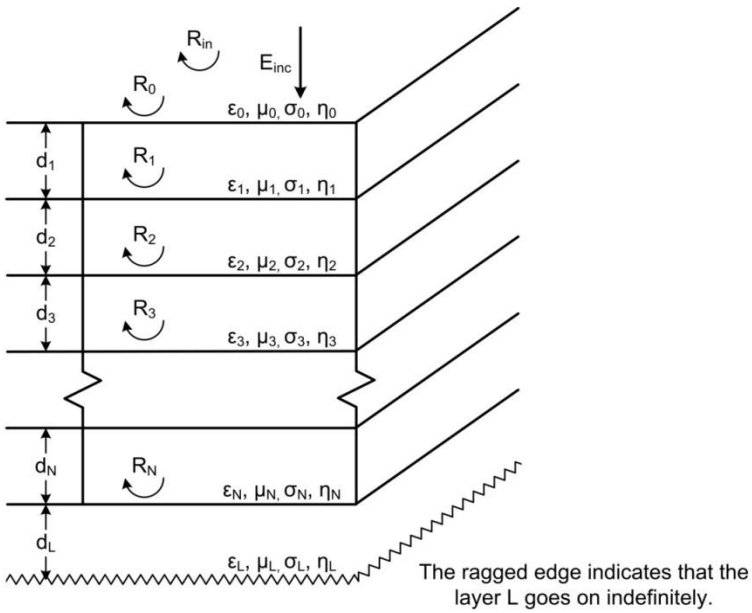

Figure 8. Multilayer structure of the ground for the multilayer analysis.

For an N-layer scenario with normal incidence the resultant reflection coefficient for a wave in air incident at the first layer is given by [4] as:

$$R_{in} = R_0 + R_1 e^{-2\gamma_1 d_1} + R_2 e^{-2(\gamma_1 d_1 + \gamma_2 d_2)} + \ldots + R_N e^{-2(\gamma_1 d_1 + \gamma_2 d_2 + \ldots + \gamma_N d_N)} \tag{3}$$

where

$$R_0 = \frac{\eta_1 - \eta_0}{\eta_1 + \eta_0} \tag{4}$$

$$R_1 = \frac{\eta_2 - \eta_1}{\eta_2 + \eta_1} \tag{5}$$

$$\begin{aligned} R_2 &= \frac{\eta_3 - \eta_2}{\eta_3 + \eta_2} \\ &\vdots \\ R_N &= \frac{\eta_L - \eta_N}{\eta_L + \eta_N} \end{aligned} \tag{6}$$

$$\eta_m = \sqrt{\frac{j\omega\mu_m}{\sigma_m + j\omega\varepsilon_m}} \tag{7}$$

$$\alpha_m = \omega\sqrt{\mu_m \varepsilon_m}\left(\frac{1}{2}\left[\sqrt{1+\left(\frac{\sigma_m}{\omega\varepsilon_m}\right)^2}-1\right]\right)^{\frac{1}{2}} \tag{8}$$

.

$$\beta_m = \omega\sqrt{\mu_m \varepsilon_m}\left(\frac{1}{2}\left[\sqrt{1+\left(\frac{\sigma_m}{\omega\varepsilon_m}\right)^2}+1\right]\right)^{\frac{1}{2}}. \tag{9}$$

$$\begin{aligned} \varepsilon_m &= \varepsilon_{rm}\varepsilon_0 \\ \mu_m &= \mu_{rm}\mu_0 \end{aligned} \tag{10}$$

$$\gamma_m = \alpha_m + j\beta_m \tag{11}$$

where

η_m is the intrinsic impedance of layer m;
α_m is the attenuation constant of layer m;
β_m is the phase constant of layer m;
γ_m is the complex propagation constant of layer m;
ε_0 is the permittivity of free-space;
ε_{rm} is the relative permittivity of layer m;
ε_m is the permittivity of layer m;
μ_0 is the permeability of free-space;
μ_{rm} is the relative permeability of the layer m;
μ_m is the permeability of the layer m;
σ_m is the conductivity of layer m;
ω is the radian frequency in radians per second and equal to $2\pi f$;
f is the radio frequency in Hertz.

The approximations and background derivations made in Equations (3) through (11) to account for the transmission coefficient across each boundary are taken from [4].

Data for this first set of measurements contains measurements taken in a parking lot section in front of Building A4 at TMFS, where the measurements were taken at four positions. The parking lot has a layer of asphalt over the soil, and the asphalt layer was assumed to be flat and uniform in thickness. The frequency was stepped from 300 kHz to 6000 MHz while the antenna remained stationary at a distance of 1.5 meters above the ground surface. The equations (3) through (11) for the multilayer reflection coefficient at normal incidence were implemented in a computer code and used to generate a number of simulations with different values of layer thicknesses, d, permittivity, ε, and conductivity, σ, with the permeability, μ, fixed at μ_0. The code computes the total reflection coefficient versus frequency for a frequency range of 500 MHz to 6000 MHz. The objective was to simulate the waveform measured at the site by adjusting parameters until there was a match to the measured waveform. Many runs were made for two-

and three-layer scenarios. The most successful match was that obtained for the TMFS Building A4 parking lot using a two-layer prediction.

The soil was expected to be of sand or gravel consistency with some rock scattered throughout its extent. Figure 9 shows a plot of the measured data taken in May of 2011 and processed in June 2011 for data measured at position 4 in the Building A4 parking lot at TMFS. There is a definite indication of a two-layer reflection phenomenon occurring with the periodic variation of the waveform. The first layer below the air-to-asphalt boundary has a finite thickness believed to be in the range of 5 to 15 cm (2 to 6 inches). The air to asphalt boundary will be referred to as the first boundary. The asphalt layer was later measured physically with a ruler to be 5.1 cm (2 inches) thick. The second layer below the asphalt to soil interface boundary is assumed to be semi-infinite in thickness and will be referred to as the second boundary. The distance between the first and second boundary is a quarter-wavelength in the asphalt at the frequency represented by the difference between the nulls in the measured waveform of Figure 9. One needs to know the permittivity of the first layer to compute a quarter-wavelength in that layer. For a two-layer scenario there are five unknowns: the four dielectric constants (conductivity and permittivity) of the asphalt and soil and the thickness of the first layer. The second layer (soil) is assumed to be semi-infinite in extent. The fifth unknown is the thickness of the first layer, but that was actually measured with a ruler.

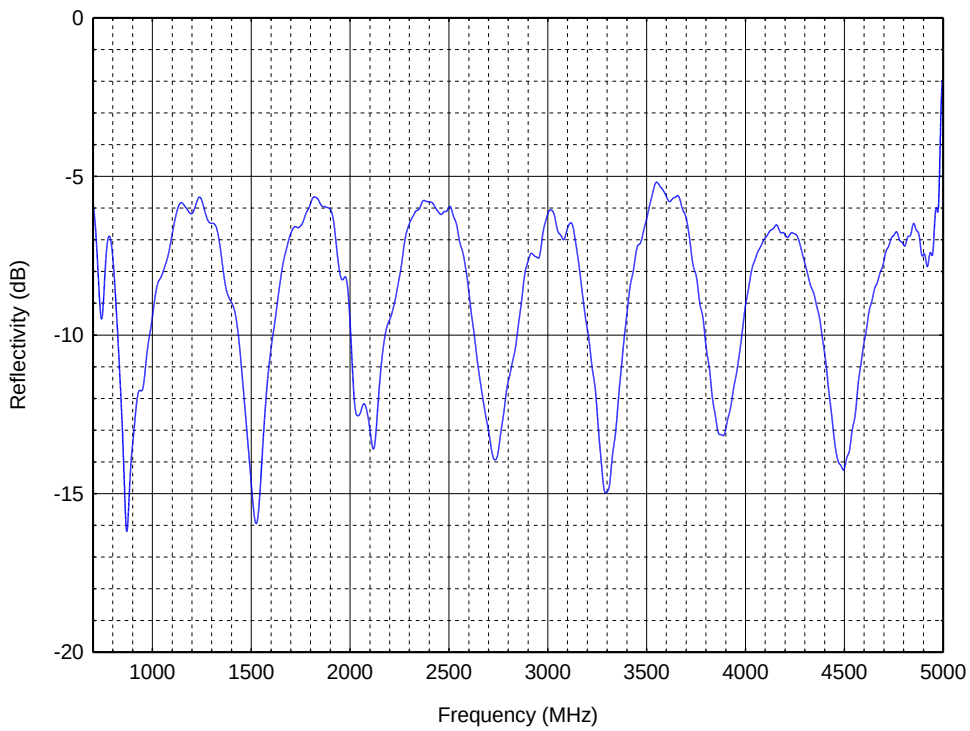

Figure 9. Measured data taken in May of 2011 for position 4 at Building A4.

Initially, a three-layer scenario was assumed, but after many runs it was difficult to come to a solution because adding a third layer to the two-layer scenario adds three more unknown variables to the five unknown variables of the two-layer scenario. Examination of the time domain deconvolved impulse response envelope obtained with a Hilbert Transformation plot

(Figure 10) shows that a definite two-layer ground structure exists at the Building A4 parking lot. The first impulse at 10 nanoseconds is the reflection from the air/ground boundary at the surface of the soil. The impulse at approximately 11.7 nanoseconds is the reflection from the boundary between layer 1 and layer 2. Since there was no discernible third impulse seen in the data, the analysis was performed under the assumption of two-layers.

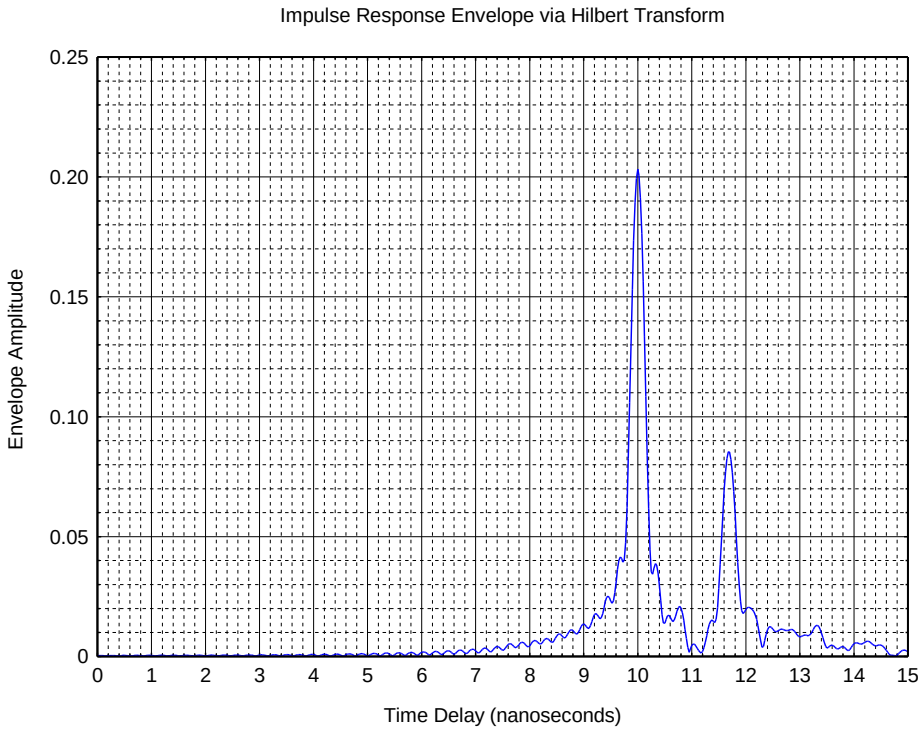

Figure 10. The deconvolved impulse response envelope from measured data obtained from a Hilbert Transformation for position 4 at Building A4.

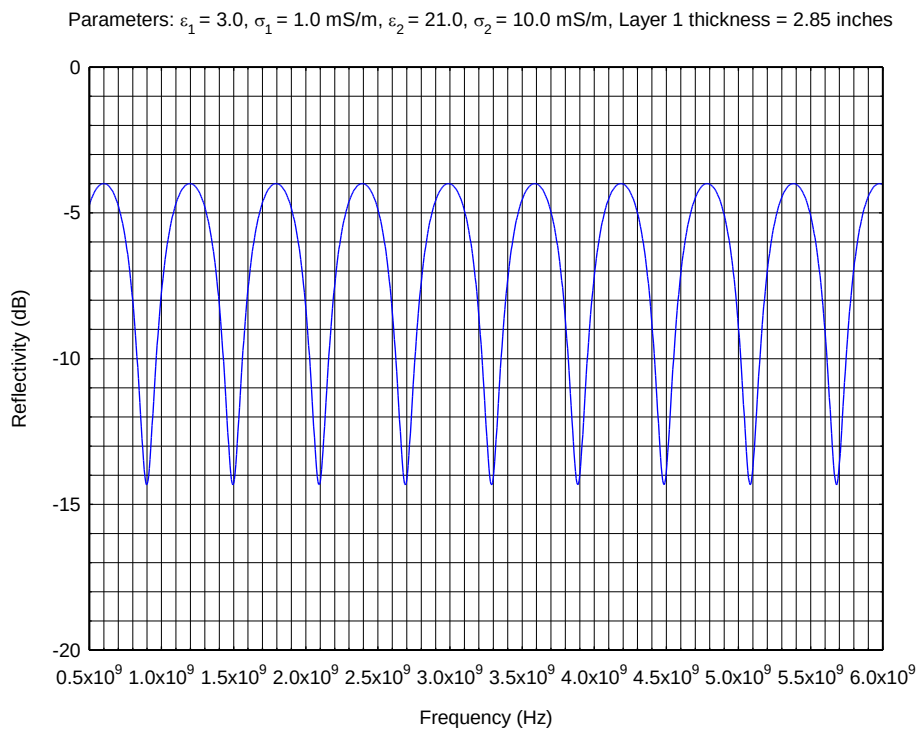

Figure 11. A plot from the multilayer prediction model that almost matches the measured data waveform of Figure 9.

Before the actual thickness of the first layer was known by direct dimensional metrology (measuring an extracted sample with a ruler), an initial guess was made that it might be around 5 to 15 cm (2 to 6 inches). Numerous simulations were performed using the computer code implementation of (3) through (11) with different values of dielectric constants and first layer thicknesses in a variation of parameters study. The parameters that were varied included the permittivity, conductivity, first-layer thickness, and the frequency. The multilayer computer model developed by ITS was run with many combinations of parameters and the reflectivity versus frequency was plotted with a separate graphics program. When the relative dielectric constant of asphalt was assumed to be 3.0, the results appeared to converge to a thickness of 7.2 cm (2.85 inches). Figure 11 shows the results for the plot that appears to approximately match the measured data plot with peak-to-peak amplitude (10 to 11 dB) and the frequency difference (600 MHz) between nulls for a 2.85 inch first layer thickness. Absolute amplitude of the peaks was difficult to match, because the losses in the asphalt/soil structure were low and there is an insensitivity to values of conductivity in the reflection coefficient at these frequencies [6],[7]. Similarly, comparison of Figure 11 (with second layer conductivity of 10.0 mS/m) to Figure 12 (with second layer conductivity of 100.0 mS/m) demonstrates how insensitive the reflection coefficient is to variations in conductivity of the second layer. Comparison of Figure 11 (with first layer conductivity of 1.0 mS/m) to Figure 13 (with first layer conductivity of 0.1mS/m) shows how insensitive the reflection coefficient of the first layer is to variations in conductivity of the first layer.

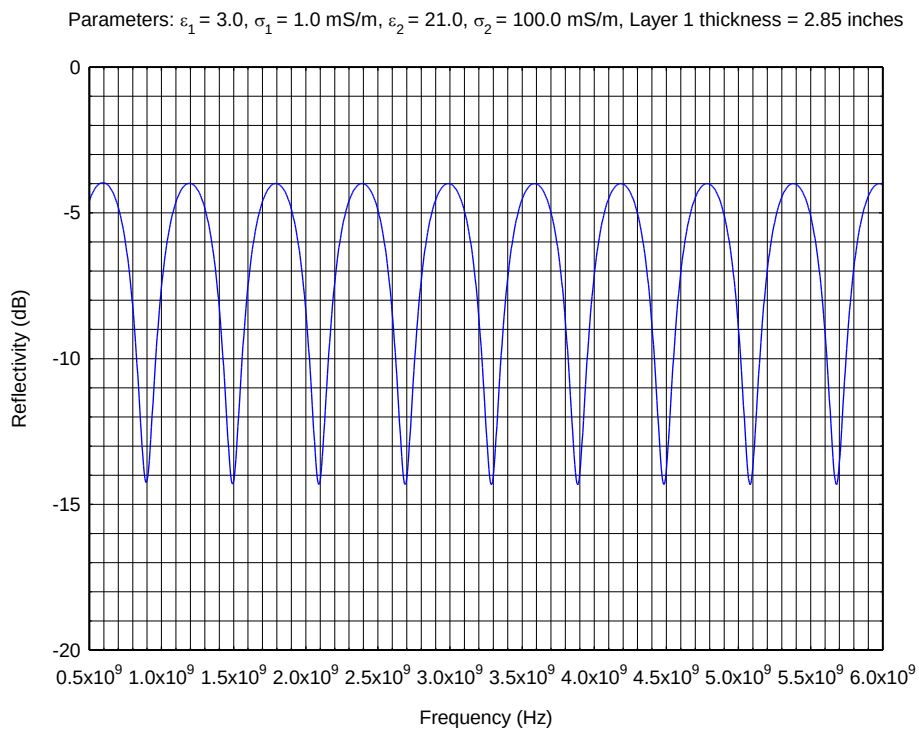

Figure 12. A plot from the multilayer prediction model that compares to Figure 11 and shows insensitivity to changes in conductivity, σ, of the second layer.

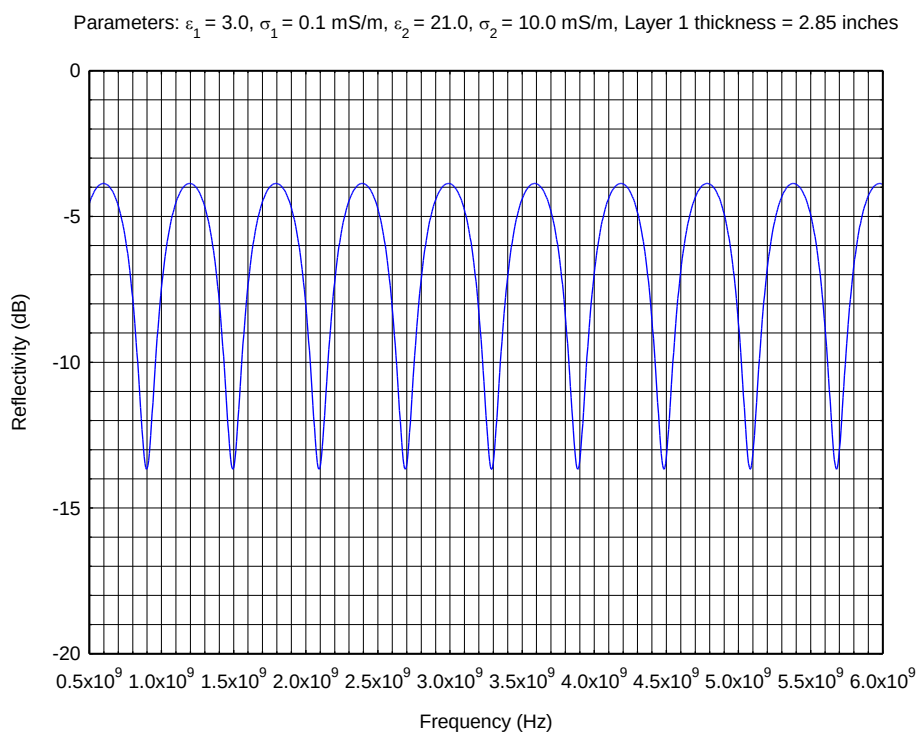

Figure 13. A plot from the multilayer prediction model that compares to Figure 11 and shows insensitivity to changes in conductivity, σ, of the first layer.

After the actual thickness of the first layer (asphalt) was physically measured with a ruler to be 5.1 cm (2 inches), then a different computation could be made using the null-to-null frequency difference frequency to determine the relative permittivity of the first layer. Using the equations for a quarter-wavelength in free space:

$$0.25\lambda_{fs} = 0.25\left({3 \times 10^8 m/sec}/{600 \times 10^6 MHz}\right) = 0.125\ meters,$$

and a quarter-wavelength in the asphalt:

$$\sqrt{\varepsilon_r} = {0.25\lambda_{fs}}/{0.25\lambda_d} = {.125}/{0.051} = 2.449\ ,$$

and solving for ε_r results in a value of 6.00 for the relative permittivity of the first layer. Figure 14 shows the predicted reflection levels for the first layer thickness of 0.051 meters (2 inches) and first layer relative permittivity of 6.0. The difference between nulls is 600 MHz. The conductivities of the first layer and second layers were assumed to be 1.0 mS/m and 10.0 mS/m, respectively. The reflectivity was found to be insensitive to the conductivities of the first and second layers.

Further simulations of the multilayer computer model (Equations (3) through (11)) were performed using parameter variation to determine the relative permittivity of the second layer (soil); it was found to be equal to 18.0. Variation of the permittivity of the second layer appears to adjust the peak-to-peak excursion of the waveform. Figure 14 is the best match to the measured waveform. A definitive result for the conductivities was not established, because of the insensitivity of the reflection coefficient to the conductivities of the layers. A different method needs to be used to measure the conductivities, as described in [6]. Comparison of the absolute level of the measured reflections of Figure 9 with those of Figure 14 shows that there is a difference in absolute magnitude. Section 4 describes the concepts of losses and skin depth to explain why these two figures may not match up exactly with respect to absolute magnitude.

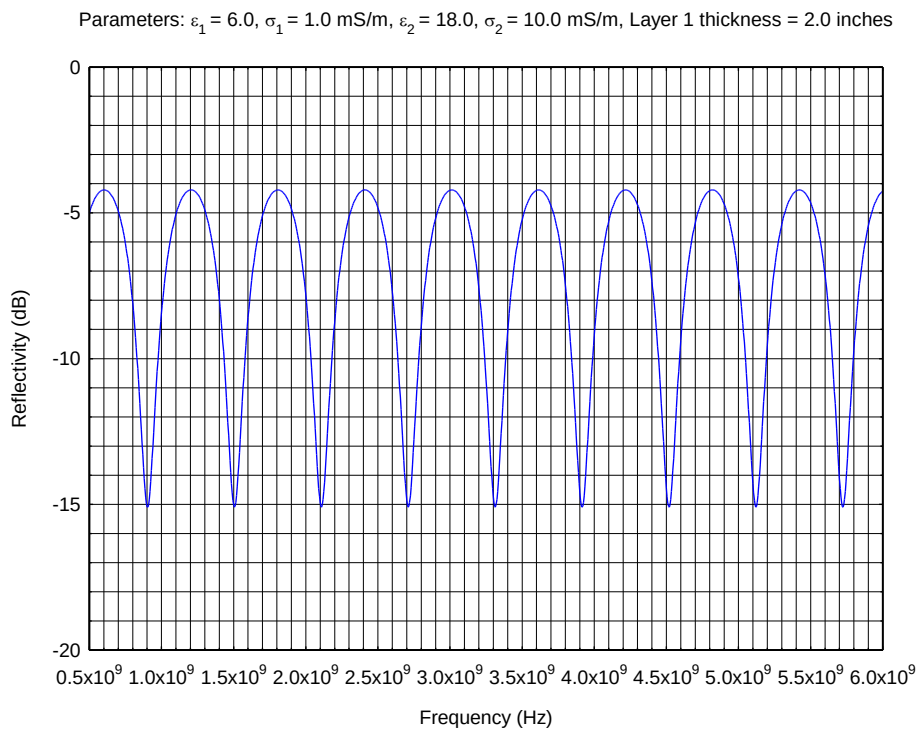

Figure 14. Final plot from the multilayer prediction model with parameters for a 5.1 cm (2 inch) asphalt actual layer thickness.

The reflection coefficient was measured at four positions at the parking lot of Building A4 that are identified in Figure 15. To the casual observer, these other positions appeared to be indistinguishable in terms of flatness and asphalt composition from Position 4, aside from location. The fact that appearances can deceive is evident in the measured reflection coefficients, which differ considerably in comparison to Figure 11. In particular, at these locations the well-defined quarter-wave nulls in the reflection coefficients are diminished to the point of being almost indistinguishable (Figure 16). Plots of the deconvolved impulse responses show that the first impulse is nearly identical at all positions, which would suggest that differences in the constitutive properties of the asphalt layer are not the culprits giving rise to the different results (Figure 17). The second impulses (in time) are quite different, however, which suggests that the constitutive properties of the substrates and/or the second interface boundaries differ considerably at Positions 1, 2, and 3 compared to Position 4 identified in Figure 15. In particular, if the second interface is roughly on the scale of a wavelength, then this can produce diffuse (non-specular) reflection at this interface. The measurements at all four locations were repeatable.

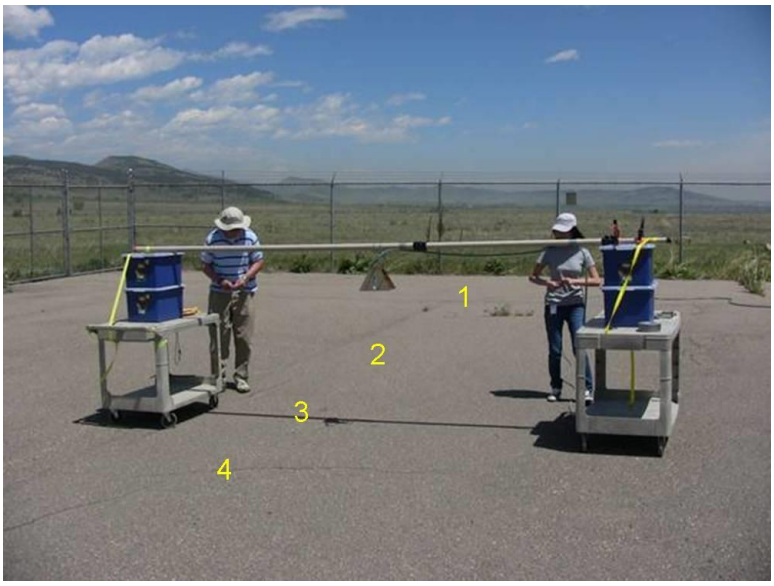

Figure 15. Measurement setup for Building A4 parking lot with location of Positions 1, 2, 3, and 4.

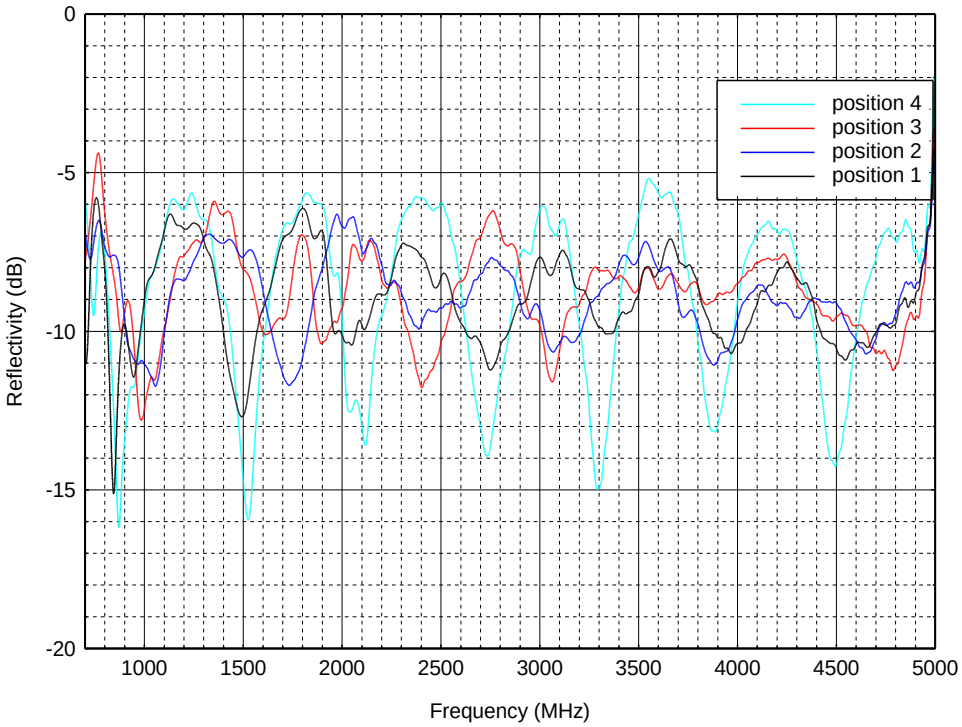

Figure 16. Reflectivity measurement for four positions at Table Mountain Building A4 parking lot.

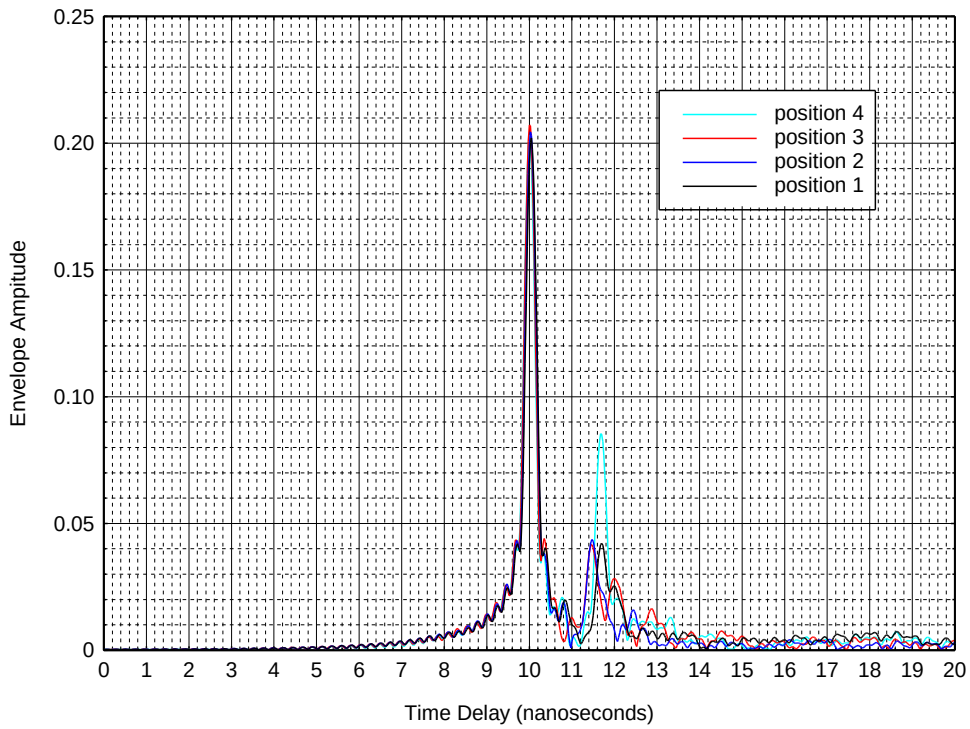

Figure 17. Impulse response envelope obtained from Hilbert Transform for four positions at Table Mountain Building A4 parking lot.

The multilayer model (Equations (3) through (11)) was used to look at a single layer where the measured data at Plateau Road indicated that the structure of the ground was a single layer. Figure 18 shows the reflectivity measurement obtained in the middle of Plateau Road. There is no definite structure of nulls and peaks as in the multilayer structure discussed previously. The ground is not homogeneous, so there is some variation in frequency, surface roughness, and irregularities. These measurements indicate a single layer structure at this particular location. Figure 19 is the corresponding impulse response for this same location showing one major impulse and indicating minimal reflection from any layers below the air/soil interface. This supports the hypothesis of a single layer.

When the ITS multilayer model is used in the single layer mode, a constant level of reflectivity versus frequency is obtained. The model was run for a variety of values of permittivity and conductivity. The reflectivity level was found to be insensitive to conductivity, but very dependent on permittivity. Figure 20 shows the reflectivity plotted as a function of relative permittivity. The average level of reflectivity in the measured data of Figure 18 above 1500 MHz is approximately -10 dB. The multilayer model computes a -10 dB level with a relative permittivity of 3.7 and a conductivity of 1.0 mS/m. The value of conductivity has no effect on this level.

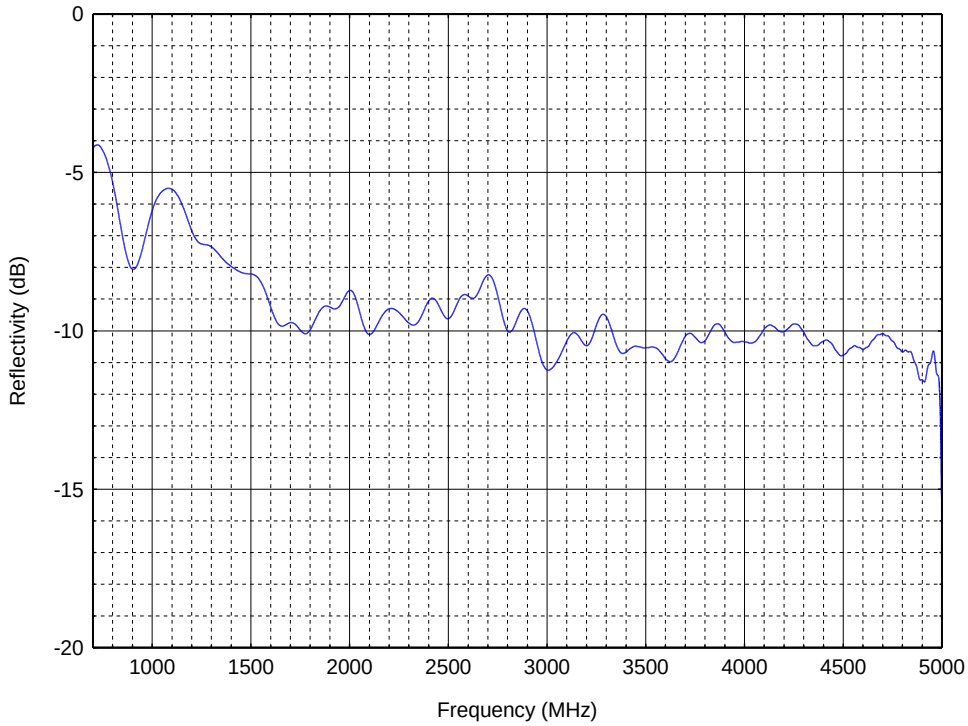

Figure 18. Measured data in the middle of Plateau Road taken in May 2010.

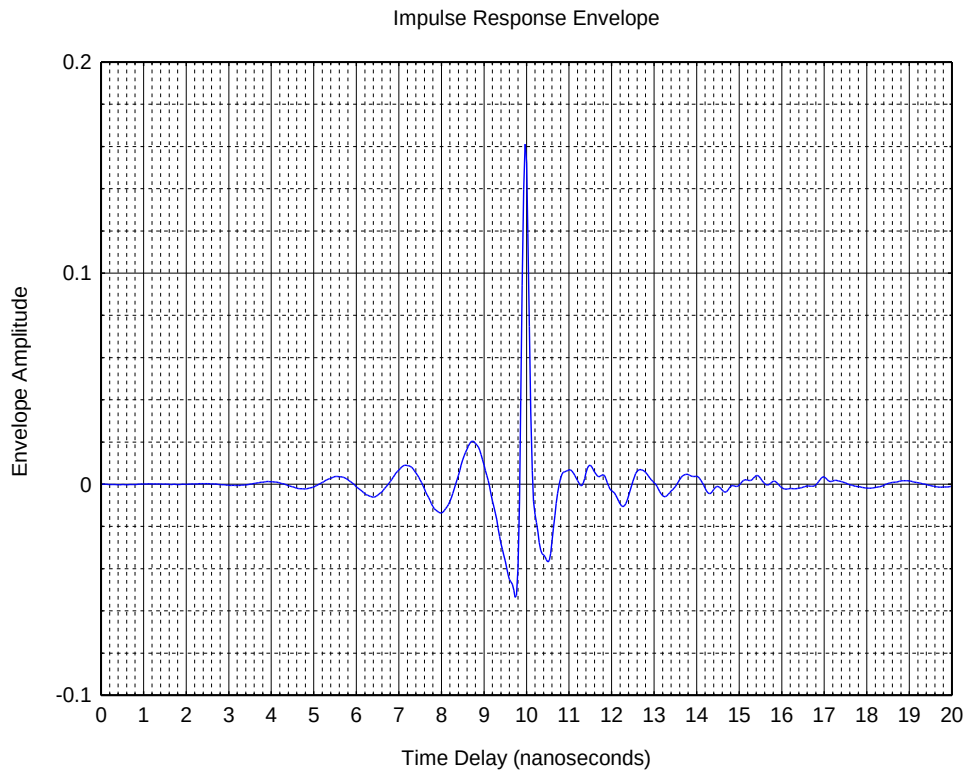

Figure 19. The deconvolved impulse response envelope from measured data in the middle of Plateau Road taken in May 2010. Note the dominant reflection from the air/ground interface.

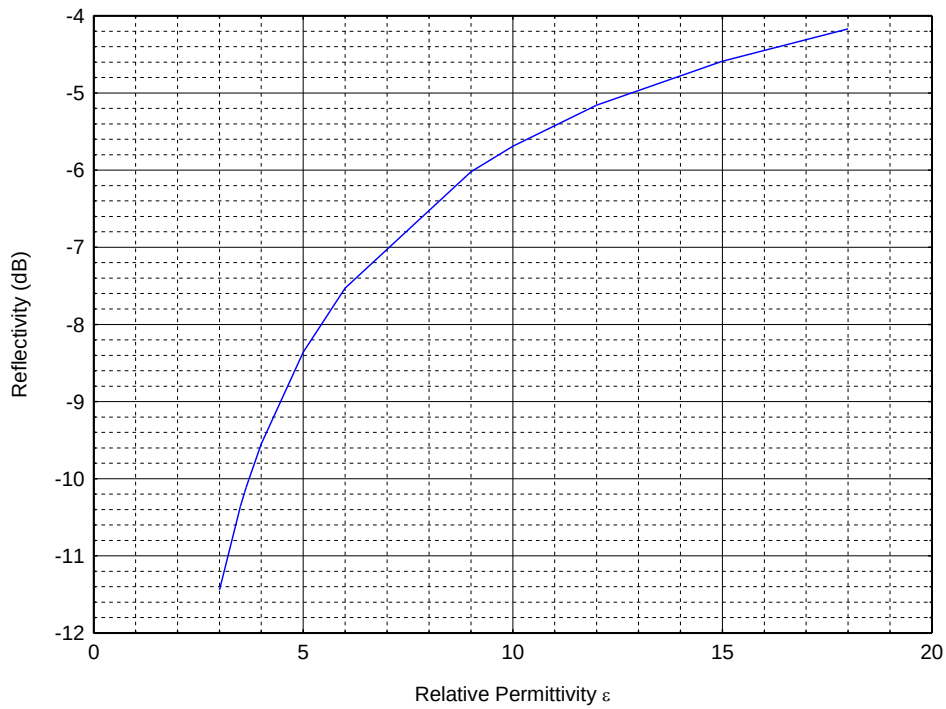

Figure 20. Predicted reflectivity versus relative permittivity ε_r of the soil using the multilayer model in single layer mode with an assumed conductivity of 1.0 mS/m.

4 ELECTRIC FIELD PENETRATION DEPTH OF THE SOIL

The purpose of this section is to explain why the magnitude of the electromagnetic wave penetrating the Earth's surface does not attenuate significantly as it passes through and returns from a reflection formed by the boundary between the first and second layer below the surface. The magnitude for the predicted and measured data of the reflection coefficient does not change as a function of ground constants and frequency due to the large magnitude of the skin depth (1 to 10 meters) for these frequencies in comparison to the magnitude for assumed and actual layer thicknesses (less than 0.1 meters) at TMFS. The skin depth does not vary significantly as a function of frequency above approximately 10 MHz.

The depth to which the ground currents and electric field penetrate below the Earth's surface and still maintain an appreciable magnitude is determined by the average values of the Earth conductivity (σ) and relative permittivity (ε_r), and the frequency. Penetration depth is similar to a skin depth phenomenon in a good conductor, but the Earth is a poor conductor. The skin depth ranges from a fraction of a meter at the highest frequencies for VHF communications to tens of meters at AM broadcast and lower frequencies. For this reason, ground-wave propagation at the lower frequencies is not particularly dependent on properties at the actual ground surface. Therefore, a recent rainfall which would result in a dramatic change of permittivity at the ground surface would not significantly affect propagation at MF and LF frequencies. However, at VHF frequencies a recent rainfall could affect the propagation of radio waves due to the additional moisture content of the ground near the ground surface.

The electric field strength at a distance z below the surface of the Earth or in general below any dielectric boundary is given by [4]:

$$E = E_0 e^{-\alpha z}, \tag{12}$$

where:

E_0 is the electric field intensity at the surface of the Earth,
z is the depth in meters below the surface of the Earth,
α is the attenuation per meter of the electric field intensity

The attenuation per meter α is given by [4]:

$$\alpha = \omega\sqrt{\mu\varepsilon}\sqrt{\frac{1}{2}\sqrt{1+\left(\frac{\sigma}{\omega\varepsilon}\right)^2} - \frac{1}{2}}, \tag{13}$$

where:

ω is the angular frequency and is equal to $2\pi f$,
f is radio frequency in Hertz,
μ is the magnetic permeability of the Earth $\mu = \mu_r \cdot 4\pi \times 10^{-7}$ Henries per meter,
μ_r is the relative permeability,
ε = the permittivity of the Earth = $\varepsilon_r \cdot (8.85 \times 10^{-12})$ Farads per meter,

ε_r is the relative permittivity of the Earth,
σ is the conductivity of the Earth in Siemens per meter.

The distance the wave must travel in a lossy medium to reduce its amplitude to e^{-1} = 0.368 of its value at the surface is $\delta = 1/\alpha$ meters and is called the skin depth of the lossy medium. For other values of attenuation of the electric field, $r=e^{-\alpha z}$, one can use α to determine the distance z below the surface where the electric field is attenuated to that ratio r. The ratio r is always less than or equal to 1. The distance z is given by:

$$z = -\frac{ln(r)}{\alpha}, \tag{14}$$

where $ln(r)$ is the natural logarithm of r.

An example is where f=300 kHz, μ_r = 1 for a nonmagnetic Earth, ε_r = 15 for average ground, σ = .005 for average ground. The attenuation α is calculated as .0751 per meter and the skin depth δ is calculated as $1/\alpha$ = 13.32 meters.

The skin depth is the distance at which the electric field is e^{-1} or 0.368 (36.8 percent) of its value at the surface of the Earth [4]. Although, the electric field at this large percentage does not represent a significant attenuation of the electric field. Some applications may require a lower electric field percentage, such as 10 percent. If the distance, z, at which the electric field is .1 (10 percent) of its value at the surface is desired, then $ln\ r$ is ln (.1) = -2.3026, and α = 0.0751, so $z = -(-2.3026)/\alpha = 30.66$ meters. Figure 21shows the skin depth of several types of media as a function of frequency. The skin depth in Figure 21 does not vary any significant amount for each media type at these frequencies. Figure 21 demonstrates how significant the different ground constants are in affecting the magnitude of the skin depth. Figure 21 shows that the skin depth is quite large for poor and average ground. Figure 22 is an expansion of Figure 21 along the frequency axis to show the skin depth in the 100 kHz to 10 MHz range, and demonstrates how large the skin depths are below 2 MHz.

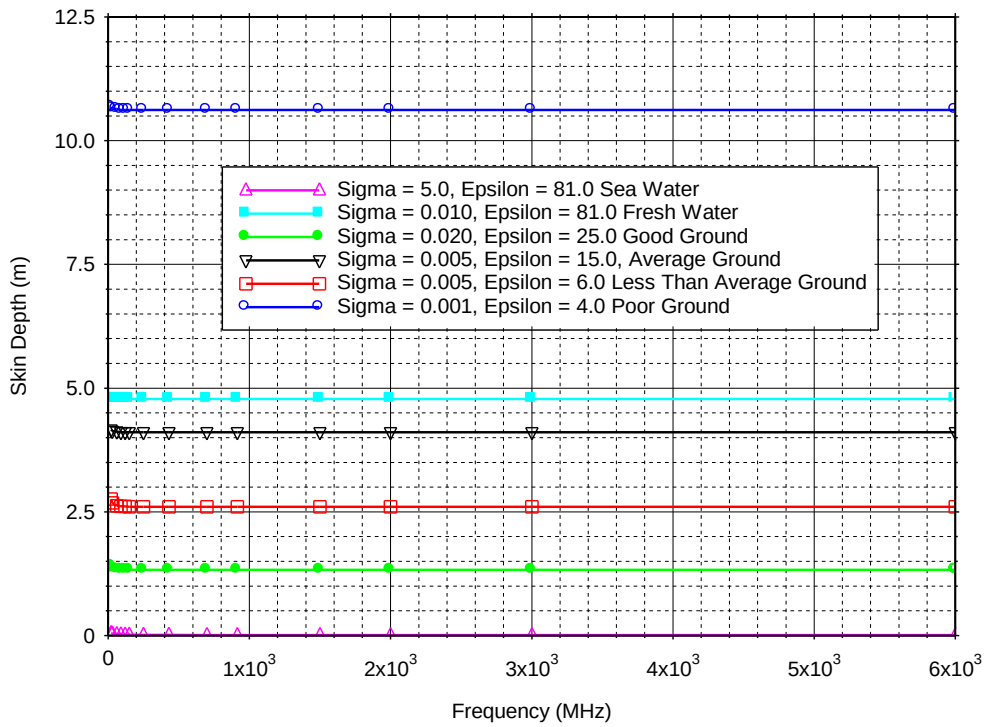

Figure 21. Skin depth for 1/*e* E-field attenuation versus frequency for various media types.

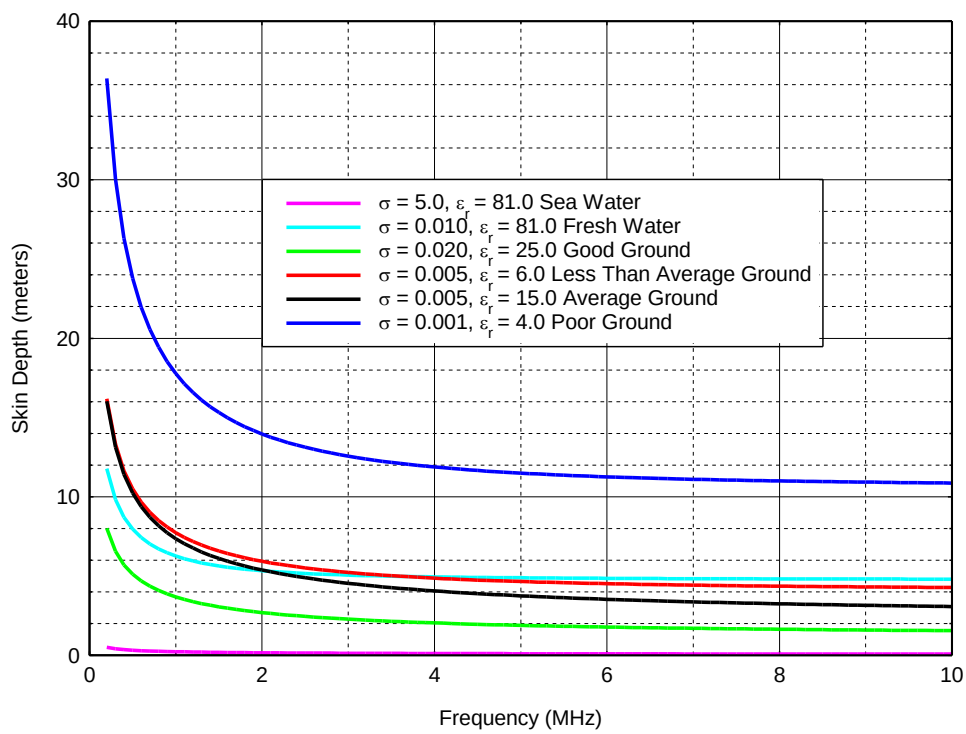

Figure 22. Skin depth for 1/*e* E-field attenuation versus frequency for various media types expanded to show lower frequencies.

5 CONCLUSIONS

The multilayer approach to analyzing the data from the reflection coefficient measurements at the Table Mountain Field Site was able to determine the dielectric constant of the soil for a two-layer analysis, but analysis with the multilayer model showed negligible change in the reflectivity when the conductivity of both layers was varied. Runs with the multilayer model have demonstrated that the reflection coefficient is relatively insensitive to changes in the conductivity even with changes of one order of magnitude. Runs that were performed with the multilayer model in attempts to recreate the measured reflectivity waveform of Figure 9 have determined that the reflectivity is primarily a function of the permittivity of the two layers and the thickness of the first layer. The distance between nulls along the frequency axis of the reflectivity plots was found to be a function of the permittivity and thickness of the first layer. The permittivity of the second layer adjusts the null depth of the reflectivity characteristics.

The permittivity of the asphalt layer for the parking lot at Building A4 was determined by measurement to be 6.0, which is in agreement with some of the values of permittivity quoted in [8] that varied from 4.5 to 6.5, depending on the specific composition of the measured samples. The determination of the permittivity for a single layer of soil was calculated from the measured reflectivity data at Plateau Road and found to vary along the length of the road. The relative permittivity at our sample location along Plateau Road was estimated to be 3.7. Our measurements indicated that this was predominantly a single layer, but with some variations in reflectivity due to the inhomogeneous nature of the soil.

6 REFERENCES

[1] R.T. Johnk et al., "Time domain measurements of the electromagnetic backscatter of pyramidal absorbers and metallic plates," IEEE Trans. EMC, Vol. 35, No. 4, November 1993.

[2] R.T. Johnk et al., Using joint time-frequency analysis to enhance time-domain numerical simulation," Interference Technology, 2003.

[3] N.S. Nahman and M.E. Guillaume, "Deconvolution of time-domain waveforms in the presence of noise," National Bureau of Standards (U.S.) Tech. Note (1047), 1981.

[4] C.A. Balanis, Advanced Engineering Electromagnetics, New York: John Wiley and Sons, 1989, pp.145–154 and pp. 220-230.

[5] E.C. Jordan, Electromagnetic Waves and Radiating Systems, New Jersey: Prentice Hall, 1968, pp.628–650.

[6] N. DeMinco et. al., "Free-field measurements of the electrical properties of soil using the surface wave propagation between two monopole antennas," NTIA Report TR-12-484, January 2012.

[7] International Telecommunications Union (ITU-R), "Electrical characteristics of the surface of the Earth," ITU-R Recommendation P.527-3, 1992.

[8] T. Saarenketo, "Electrical properties of road materials and subgrade soils and the use of ground penetrating radar in traffic infrastructure surveys," PhD Thesis, Faculty of Science, Department of Geoscience of the University of Oulu, Finland, Oulu University Press, Nov. 11, 2006.

FORM **NTIA-29**
(4-80)

U.S. DEPARTMENT OF COMMERCE
NAT'L. TELECOMMUNICATIONS AND INFORMATION ADMINISTRATION

BIBLIOGRAPHIC DATA SHEET

1. PUBLICATION NO. TR-13-494	2. Government Accession No.	3. Recipient's Accession No.
4. TITLE AND SUBTITLE Free-Field Measurements of the Electrical Properties of Soil Using the Measured Reflection Coefficient at Vertical Incidence and Multilayer Analysis		5. Publication Date September 2012 6. Performing Organization Code NTIA/ITS
7. AUTHOR(S) Paul M. McKenna, Nicholas DeMinco, Robert T. Johnk, Chriss A. Hammerschmidt, J. Wayde Allen		9. Project/Task/Work Unit No. 3155000-300
8. PERFORMING ORGANIZATION NAME AND ADDRESS Institute for Telecommunication Sciences National Telecommunications & Information Administration U.S. Department of Commerce 325 Broadway Boulder, CO 80305		10. Contract/Grant Number.
11. Sponsoring Organization Name and Address Table Mountain Research Project Institute for Telecommunication Sciences National Telecommunications & Information Administration U.S. Department of Commerce 325 Broadway Boulder, CO 80305		12. Type of Report and Period Covered
14. SUPPLEMENTARY NOTES		

15. ABSTRACT (A 200-word or less factual summary of most significant information. If document includes a significant bibliography or literature survey, mention it here.)

This report describes a free-field radio frequency (RF) measurement system that is currently being developed by engineers at the Institute for Telecommunication Sciences (NTIA/ITS). The objective is to provide estimates of the electrical properties of the ground (permittivity and conductivity) over which the measurement system is deployed. This measurement system uses reflection coefficient measurements at vertical incidence over ground using a dual-ridged horn antenna placed close to and radiating directly down at the ground at specific antenna heights. Soil properties are extracted by comparing measured data with known analytical models for single and multilayer scenarios using optimization.

16. Key Words (Alphabetical order, separated by semicolons)

17. AVAILABILITY STATEMENT ☒ UNLIMITED. ☐ FOR OFFICIAL DISTRIBUTION.	18. Security Class. (This report) Unclassified 19. Security Class. (This page) Unclassified	20. Number of pages 39 21. Price:

NTIA FORMAL PUBLICATION SERIES

NTIA MONOGRAPH (MG)

A scholarly, professionally oriented publication dealing with state-of-the-art research or an authoritative treatment of a broad area. Expected to have long-lasting value.

NTIA SPECIAL PUBLICATION (SP)

Conference proceedings, bibliographies, selected speeches, course and instructional materials, directories, and major studies mandated by Congress.

NTIA REPORT (TR)

Important contributions to existing knowledge of less breadth than a monograph, such as results of completed projects and major activities. Subsets of this series include:

NTIA RESTRICTED REPORT (RR)

Contributions that are limited in distribution because of national security classification or Departmental constraints.

NTIA CONTRACTOR REPORT (CR)

Information generated under an NTIA contract or grant, written by the contractor, and considered an important contribution to existing knowledge.

JOINT NTIA/OTHER-AGENCY REPORT (JR)

This report receives both local NTIA and other agency review. Both agencies' logos and report series numbering appear on the cover.

NTIA SOFTWARE & DATA PRODUCTS (SD)

Software such as programs, test data, and sound/video files. This series can be used to transfer technology to U.S. industry.

NTIA HANDBOOK (HB)

Information pertaining to technical procedures, reference and data guides, and formal user's manuals that are expected to be pertinent for a long time.

NTIA TECHNICAL MEMORANDUM (TM)

Technical information typically of less breadth than an NTIA Report. The series includes data, preliminary project results, and information for a specific, limited audience.

For information about NTIA publications, contact the NTIA/ITS Technical Publications Office at 325 Broadway, Boulder, CO, 80305 Tel. (303) 497-3572 or e-mail info@its.bldrdoc.gov.

This report is for sale by the National Technical Information Service, 5285 Port Royal Road, Springfield, VA 22161,Tel. (800) 553-6847.